Astronomy
&
Astrophysics

LETTER TO THE EDITOR

Larger λ_R in the disc of isolated active spiral galaxies than in their non-active twins

I. del Moral-Castro[1,2], B. García-Lorenzo[1,2], C. Ramos Almeida[1,2], T. Ruiz-Lara[1,2], J. Falcón-Barroso[1,2], S. F. Sánchez[3], P. Sánchez-Blázquez[4,5], I. Márquez[6], and J. Masegosa[6]

[1] Instituto de Astrofísica de Canarias, C/ Vía Láctea, s/n, 38205 La Laguna, Tenerife, Spain
e-mail: ignaciodelmoralcastro@gmail.com
[2] Departamento de Astrofísica, Universidad de La Laguna, 38206 La Laguna, Tenerife, Spain
[3] Instituto de Astronomía, Universidad Nacional Autónoma de México, A. P. 70-264, 04510 CDMX, Mexico
[4] Departamento de Física de la Tierra y Astrofísica, Universidad Complutense de Madrid, 28040 Madrid, Spain
[5] IPARCOS, Facultad de CC Físicas, Universidad Complutense de Madrid, 28040 Madrid, Spain
[6] Instituto de Astrofísica de Andalucía (CSIC), Glorieta de la Astronomía s/n, 18008 Granada, Spain

ABSTRACT

We present a comparison of the spin parameter λ_R, measured in a region dominated by the galaxy disc, between 20 pairs of nearby ($0.005 < z < 0.03$) seemingly isolated twin galaxies differing in nuclear activity. We find that $80-82\%$ of the active galaxies show higher values of λ_R than their corresponding non-active twin(s), indicating larger rotational support in the active galactic nuclei (AGN) discs. This result is driven by the 11 pairs of unbarred galaxies, for which 100% of the AGN show larger λ_R than their twins. These results can be explained by a more efficient angular momentum transfer from the inflowing gas to the disc baryonic matter in the case of the active galaxies. This gas inflow could have been induced by disc or bar instabilities, although we cannot rule out minor mergers if these are prevalent in our active galaxies. This result represents the first evidence of galaxy-scale differences between the dynamics of active and non-active isolated spiral galaxies of intermediate stellar masses ($10^{10} < M_* < 10^{11} M_\odot$) in the Universe.

Key words. galaxies: active – galaxies: nuclei – galaxies: kinematics and dynamics

1. Introduction

Observational evidence suggests a co-evolution of the central supermassive black holes (SMBHs; see Ho 2008 for a review) and their host galaxies (see e.g. Kormendy & Ho 2013). Unveiling the mechanism(s) controlling this co-evolution is crucial to improve our understanding of the formation and evolution of galaxies. Active galactic nuclei (AGN) feedback has been proposed as the main mechanism regulating SMBH and galaxy growth in massive galaxies, and it can act in different ways (e.g. Fabian 2012). Understanding how nuclear activity is triggered and whether all massive galaxies go through an active phase is then of great importance. Significant observational effort has been made to observe the closest environment of SMBHs in order to study AGN fuelling (e.g. García-Burillo et al. 2005; Ramos Almeida & Ricci 2017; Storchi-Bergmann & Schnorr-Müller 2019 and references therein). To induce inflows of gas towards the galactic centre, the gas in the host galaxy has to lose angular momentum, but the dominant mechanism(s) that transport the gas from galaxy scales to the central parsecs in AGN are not clear yet (Alexander & Hickox 2012). In this respect, the definition of non-active samples is essential to search for properties that might be unique to AGN. Legacy integral field spectroscopy (IFS) surveys such as ATLAS[3D] (Cappellari et al. 2011), CALIFA (Sánchez et al. 2012), SAMI (Croom et al. 2012), MASSIVE (Ma et al. 2014), or MaNGA (Bundy et al. 2015) now provide

the opportunity to select almost identical pairs of galaxies differing only in nuclear activity. By comparing the kinematic properties of these pairs it should be possible to spot differences connected to AGN triggering (del Moral-Castro et al. 2019, hereafter dMC19).

An effective way to quantify the global velocity structure of galaxies taking advantage of IFS is λ_R (Emsellem et al. 2007). This dimensionless spin parameter permits us to assess the rotational support of a galaxy, similarly to V/σ, and it goes to unity when rotation dominates. Thanks to the previously mentioned IFS surveys it has been possible to study λ_R for a large number of galaxies covering a wide range of morphological types and stellar masses (Cappellari 2016; Colless 2018). These data have been used to look for dependences with different global galaxy properties. For example, Krajnović et al. (2013) studied a sample of early-type galaxies from ATLAS[3D] and found that λ_R decreases with increasing bulge fraction. This dependence was confirmed for a wider range of galaxy morphologies by Falcón-Barroso et al. (2019) using data from CALIFA. An anti-correlation between λ_R (or V/σ) and stellar mass (M_*) has also been reported using data from MASSIVE and ATLAS[3D] (Veale et al. 2017) along with MaNGA (Graham et al. 2018) and SAMI (van de Sande et al. 2018). It is noteworthy that none of the latter works studied possible differences in λ_R between active and non-active galaxies. A few works based on large IFS surveys comparing different properties of active and non-active galaxies have been published (e.g. Rembold et al. 2017;

Sánchez et al. 2018; Lacerda et al. 2020). In Sánchez et al. (2018), based on MaNGA data and including 98 AGN, the authors report that on average these AGN have lower rotational support (~65%) than the non-active galaxies within $1\,R_e$ (i.e. bulge-dominated). This trend is mainly driven by late-type galaxies, which dominate their AGN sample (see Fig. 2 in Sánchez et al. 2018). Ilha et al. (2019) performed a kinematic analysis of 62 AGN from MaNGA and report larger differences between σ_{gas} and σ_{stars} in the central kiloparsec of the active galaxies than in the corresponding control sample.

In dMC19 we performed a pilot study based on two low-luminosity isolated active galaxies (barred and unbarred) and their two non-active twins matched in galaxy properties using data from the CALIFA survey. Our goal was to identify large-scale differences between the twins that could be related to AGN triggering. From the analysis of this pilot sample we found that each active galaxy had larger λ_R within $1\,R_e$ and globally, internal twists in their gas discs, dynamical lopsidedness, and older stellar populations in the central kiloparsec of the galaxy than its corresponding non-active twin. In view of these results, we decided to extend this study to a larger sample of twin galaxies differing in nuclear activity selected from CALIFA. This is the first work focussed on studying the differences in stellar λ_R between active and non-active galaxies matched in galaxy properties and based on one-to-one comparisons. In the following we assume a standard ΛCDM model with $H_0 = 71\,\mathrm{km\,s^{-1}\,Mpc^{-1}}$, $\Omega_m = 0.27$ and $\Omega_\Omega = 0.73$.

2. Observations and sample selection

We used data from the third data release (Sánchez et al. 2016) of the CALIFA survey (Sánchez et al. 2012), which corresponds to 667 galaxies in the Local Universe ($0.005 < z < 0.03$). Méndez-Abreu et al. (2017) selected 404 of these galaxies to characterise their 2D morphology, discarding interacting systems, mergers, and highly inclined galaxies ($i > 70°$). This is the parent sample of this work. We used the fully reduced COMBO data cubes, which are a combination of those obtained with the V500 (wavelength range 3745−7500 Å, $R \sim 850$) and V1200 (3700−4840 Å, $R \sim 1650$) gratings. We do not have COMBO data cubes for two of the galaxies and we used the V500 instead. Details on the observational strategy, data quality, data reduction, and statistical properties of the CALIFA survey can be found in Sánchez et al. (2012, 2016), Walcher et al. (2014) and García-Benito et al. (2015).

In order to identify isolated galaxies in CALIFA we followed the criteria of Barrera-Ballesteros et al. (2014). We discarded galaxies having companions with similar systemic velocity (absolute difference smaller than $1000\,\mathrm{km\,s^{-1}}$) and SDSS r-band magnitudes (within 2 mag) within a physical radius of 250 kpc. By doing this we discard major mergers and interactions, but we cannot rule out the presence of minor mergers.

To select our AGN sample we first used the codes pPXF (Cappellari & Emsellem 2004; Cappellari 2017) and GANDALF (Sarzi et al. 2006; Falcón-Barroso et al. 2006) to characterise the emission line profiles of the central spaxel of each galaxy. We consider as AGN candidates all the objects above the Kewley et al. (2001) demarcation curve in the three classical BPT diagrams (Baldwin et al. 1981) that lie in the Seyfert region of the [OIII]/[OII] versus [NII]/Hα diagram (Cid Fernandes et al. 2010). Using these criteria we identified 19 isolated active galaxies with Hubble types from Sa/SBa to Sbc/SBbc. In this work, we focus on spiral galaxies because we are interested in the study of λ_R of the stars in the disc

component (see Sect. 3 for further details). These galaxies are low-luminosity AGN, making them ideal candidates to look for triggering imprints and characterise the stellar populations of their host galaxies.

For each AGN we then selected a control sample of non-active galaxies with similar galaxy properties (twin galaxies). By doing this any possible difference between the twins should be associated with nuclear activity. We matched the twins in Hubble type, stellar mass (M_*), absolute magnitude in the r band (M_R), and disc ellipticity in the r band (ϵ). Absolute differences are smaller than $0.25 \log(M_*/M_\odot)$, 0.70 mag, and 0.20, respectively (see Table 1). Applying these criteria we did not find a twin for 5 of the 19 active galaxies. In the case of the barred active galaxies we selected twins with bar radius differences below 3 kpc. With this restriction we have another 3 AGN lacking of twins. This leaves us with a final sample of 11 active spiral galaxies (10 type 2 and 1 type 1 AGN), of which 5 are barred and 6 unbarred.

Finally, we visually inspected the SDSS images of each active galaxy and its corresponding twin candidates to select the most similar one (best twin hereafter; see Fig. 1 for an example) and discarded only those that clearly have different appearances. After doing this we end up with 5 AGN with 2 or more non-active twins. In these cases, we always identified the best twin but we did not discard the others. Furthermore, 5 non-active galaxies are selected as twins of 2 different AGN. In total we have 20 pairs of isolated twin galaxies differing in nuclear activity (see Table 1 and Appendix A).

3. Methodology

The stellar kinematics were calculated following the same methodology as in dMC19. We removed all the spaxels with $S/N < 3$ and spatially binned the spaxels using the Voronoi 2D binning method (Cappellari & Copin 2003) to achieve S/N of ~30. We used pPXF to fit the 3800−7000 Å spectral range. Finally, λ_R was measured as in Emsellem et al. (2007) as follows:

$$\lambda_R \equiv \frac{\langle R|V|\rangle}{\langle R\sqrt{V^2 + \sigma^2}\rangle} = \frac{\sum_{i=1}^{N_p} F_i R_i |V_i|}{\sum_{i=1}^{N_p} F_i R_i \sqrt{V_i^2 + \sigma_i^2}}, \qquad (1)$$

where R_i, F_i, V_i, and σ_i are the distance to the centre, flux, stellar velocity, and velocity dispersion per spatial bin i.

λ_R is usually calculated within one effective radius or radially (see e.g. Falcón-Barroso et al. 2019 and references therein). By comparing the stellar λ_R radial profiles of the two AGN and their non-active twins, in dMC19 we found the largest differences in the galaxy discs. Furthermore, the interpretation given in dMC19 to explain the differences in λ_R between twin galaxies differing in nuclear activity also suggested that we focus on the region dominated by the disc (see Sect. 4). To identify this region in each galaxy we used the 2D photometric decomposition from Méndez-Abreu et al. (2017). This way we can determine the radius at which the intersection between the bulge and disc profiles happens. We find that this radius is never larger than two times the bulge effective radius (R_e^{bul}). Therefore, we can select $2\,R_e^{bul}$ as the inner radius of the region where the disc component dominates over the bulge for all the galaxies in the sample. To determine the disc outer radius (R_{out}) we have to consider the extent of the galaxies in the CALIFA data. We define

Table 1. Sample properties.

AGN Twin	Type	D_L (Mpc)	Scale (pc/″)	$\log(M_*/M_\odot)$	M_R (mag)	ϵ	r_{bar} (kpc)	R_e^{bul} (kpc)	R_e (kpc)	R_{out} (kpc)	λ_R	λ_R^d
(1)	(2)	(3)	(4)	(5)	(6)	(7)	(8)	(9)	(10)	(11)	(12)	(13)
NGC 0214	SBbc	62	301	10.73	−21.93	0.31	5.4	0.5	5.5	8.1	0.72	0.76 ± 0.02
NGC 2253	SBbc	53	257	10.50	−21.34	0.21	3.9	0.3	4.0	8.7	0.53	0.61 ± 0.03
NGC 1093	SBbc	72	349	10.43	−21.29	0.34	6.6	1.8	4.8	10.1	0.64	0.68 ± 0.02
NGC 5947*	SBbc	83	402	10.56	−21.16	0.18	6.4	0.5	5.0	12.1	0.58	0.67 ± 0.03
NGC 6004	SBbc	62	301	10.63	−21.41	0.18	9.0	0.3	6.7	9.4	0.60	0.69 ± 0.03
NGC 2253	SBbc	53	257	10.50	−21.34	0.21	3.9	0.3	4.0	8.7	0.53	0.61 ± 0.03
NGC 2540	SBbc	91	441	10.21	−21.49	0.38	7.1	0.5	6.3	12.6	0.67	0.71 ± 0.02
NGC 2410	SBb	68	330	10.86	−21.60	0.72	6.3	1.1	7.1	13.0	0.76	0.76 ± 0.01
NGC 5522	SBb	73	354	10.67	−21.33	0.65	6.7	0.5	6.0	12.7	0.75	0.76 ± 0.01
NGC 2639	Sa	51	247	11.09	−21.93	0.50	–	1.0	4.3	8.4	0.62	0.65 ± 0.01
NGC 0160	Sa	72	349	10.99	−21.86	0.49	–	2.1	7.7	11.5	0.57	0.60 ± 0.01
NGC 2906	Sbc	34	165	10.46	−20.60	0.44	–	0.3	3.2	5.9	0.73	0.75 ± 0.01
NGC 0001*	Sbc	63	305	10.58	−21.30	0.38	–	1.4	3.9	10.1	0.57	0.61 ± 0.02
NGC 6063	Sbc	48	233	10.28	−20.37	0.45	–	0.9	4.8	7.9	0.70	0.72 ± 0.01
UGC 09777	Sbc	75	364	10.25	−20.60	0.43	–	1.0	3.6	8.4	0.55	0.58 ± 0.02
NGC 2916	Sbc	57	276	10.64	−21.25	0.35	–	0.9	7.2	10.1	0.71	0.75 ± 0.02
NGC 0001*	Sbc	63	305	10.58	−21.30	0.38	–	1.4	3.9	10.1	0.57	0.61 ± 0.02
NGC 6394	SBbc	123	596	10.86	−21.79	0.59	17.9	0.6	8.7	17.0	0.82	0.83 ± 0.01
UGC 12810	SBbc	112	543	10.81	−21.76	0.61	19.6	0.6	11.2	16.3	0.80	0.81 ± 0.01
NGC 7311	Sa	64	310	10.96	−22.20	0.48	–	0.7	3.9	9.9	0.70	0.72 ± 0.01
NGC 0160	Sa	72	349	10.99	−21.86	0.49	–	2.1	7.7	11.5	0.57	0.60 ± 0.01
NGC 7466	Sbc	105	509	10.68	−21.69	0.61	–	2.0	6.9	16.3	0.78	0.79 ± 0.01
NGC 2596*	Sbc	87	422	10.87	−21.44	0.65	–	2.8	8.2	13.5	0.73	0.74 ± 0.01
NGC 5980	Sbc	66	320	10.69	−21.70	0.63	–	1.1	5.6	10.2	0.74	0.75 ± 0.01
UGC 00005	Sbc	100	485	10.74	−21.90	0.49	–	0.6	8.1	16.2	0.83	0.84 ± 0.01
NGC 2596*	Sbc	87	422	10.87	−21.44	0.65	–	2.8	8.2	13.5	0.73	0.74 ± 0.01
NGC 5980	Sbc	66	320	10.69	−21.70	0.63	–	1.1	5.6	10.2	0.74	0.75 ± 0.01
NGC 0001*	Sbc	63	305	10.58	−21.30	0.38	–	1.4	3.9	10.1	0.57	0.61 ± 0.02
UGC 03973†	SBbc	95	461	10.21	−21.61	0.16	16.6	0.8	7.9	13.8	0.45	0.56 ± 0.04
UGC 02311*	SBbc	97	470	10.43	−21.85	0.33	13.6	0.7	6.7	12.1	0.63	0.68 ± 0.02
NGC 6032	SBbc	69	335	10.42	−20.96	0.26	16.4	0.4	9.2	11.9	0.67	0.72 ± 0.02

Notes. (1) Galaxy name (non-active twin names are shifted). ∗ indicates the best twin of each AGN and † the only type 1 AGN in our sample. (2) Hubble type from Walcher et al. (2014); (3) luminosity distance; (4) spatial scale; (5) total stellar mass; (6) Petrosian magnitude from Walcher et al. (2014); (7) disc ellipticity; (8) bar radius; (9) bulge effective radius in the r band from Méndez-Abreu et al. (2017); (10) effective radius in the r band from Falcón-Barroso et al. (2017); (11) outer radius (this work); (12) projected λ_R in the region dominated by the disc, with maximum associated errors of 0.01; and (13) deprojected λ_R and the corresponding error.

R_{out} as the radius of the outermost ellipse without empty spaxels/voxels (see Table 1 and Fig. 1). Thus, we used the annular region between $2 R_e^{bul}$ and R_{out} to calculate λ_R in the disc[1].

In order to calculate uncertainties we used Monte Carlo simulations, adding the corresponding errors of the CALIFA data cubes to the spectrum of each voxel following a Gaussian distribution. The procedure was repeated 100 times, resulting in 100 different λ_R values. The standard deviation of this distribution of values is our statistical error, which is always smaller than 0.01. In the following we consider 0.01 as the error of each λ_R.

4. Results and discussion

Figure 2 shows the differences in λ_R of the disc ($\Delta\lambda_R$) between each AGN and its twin(s). Considering only the best twins (indi-

[1] For NGC 2540, Méndez-Abreu et al. (2017) did not include a bulge in their photometric decomposition, but a nuclear point source. We thus estimated R_e^{bul} using the average ratio of R_{out}/R_e^{bul} of all the galaxies with the same morphological type (SBbc) in our sample.

cated with green circles in Fig. 2), we find 9/11 (82%) pairs in which the active galaxy has higher λ_R than its twin. If we consider the 20 pairs of galaxies the percentage is similar: 16/20 (80%) have $\Delta\lambda_R > 0.01$ (i.e. larger than the corresponding error). The case of UGC 03973, the only type 1 AGN in our sample, is noteworthy because it has considerably lower λ_R than its two twins. This could be related to nuclear contamination of the central spaxels associated with the large point spread function (PSF) size of the CALIFA data. It is worth mentioning, however, that using a sample of 98 AGN from MaNGA, Sánchez et al. (2018) report a tendency of type 1 AGN to be hosted in more massive, centrally concentrated and pressure-supported galaxies (within $1 R_e$) than type 2 AGN. If these results are confirmed it would provide support to an evolutionary transition between types rather than mere orientation-based differences. A larger AGN sample is required to investigate whether type 1 AGN have different kinematics than type 2 AGN.

As we mentioned in Sect. 2, we have 5 barred AGN and 6 without bars. If we only consider the unbarred galaxies in our sample, we find that 11/11 pairs (100%) show $\Delta\lambda_R > 0.01$. In
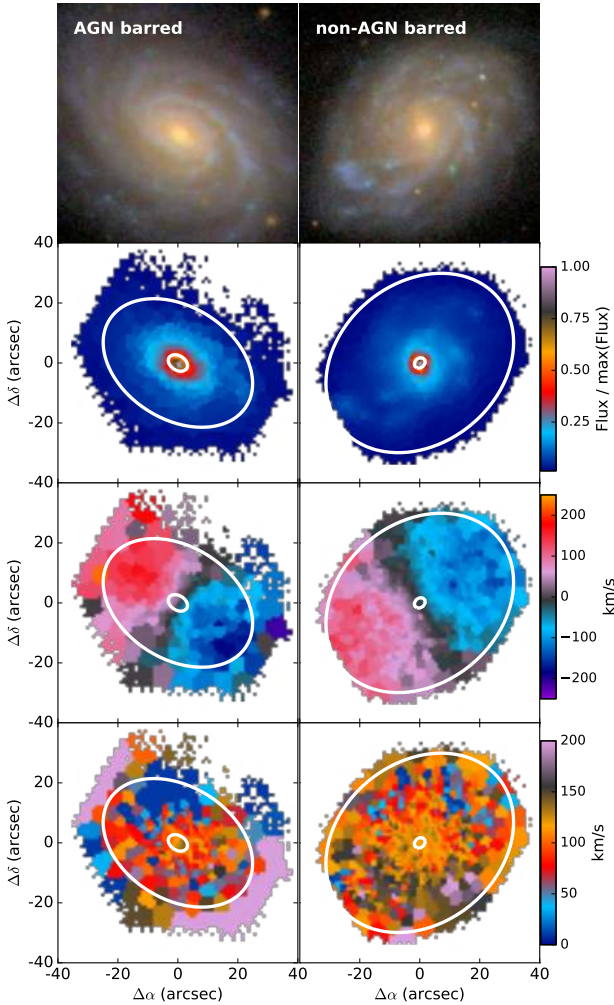
Fig. 1. Colour-composite SDSS images and CALIFA stellar flux, velocity, and velocity dispersion maps (*from top to bottom*) of one pair of twin galaxies: NGC 0214 (AGN; *left column*) and NGC 2253 (non-AGN; *right column*). The white ellipses indicate the boundaries of disc region defined in Sect. 3 ($2 R_{\rm e}^{\rm bul} \leq R_i \leq R_{\rm out}$).

the case of the barred galaxies, we have 5/9 pairs (56%), 5/7 (71%) if we do not consider the type 1 AGN.

λ_R is derived from projected quantities and therefore it depends on the viewing angle (Emsellem et al. 2007). However, for our twins the effect of galaxy inclination on $\Delta\lambda_R$ should be small because we matched them in disc ellipticity (ϵ). In Fig. 2 we show with different colours the differences in ellipticity ($\Delta\epsilon$) between each AGN and its corresponding twin(s), which are always smaller than 0.2 (see Sect. 2). Seven active galaxies have higher ϵ than their twins (i.e. more inclined, seven have lower ϵ, and four are almost identical. Thus, the slightly different inclinations between twins would not be driving the difference in λ_R. To further confirm this, we deprojected the individual λ_R values as described in Appendix B. Considering these values and their corresponding errors (see Table 1), the percentage of AGN having larger λ_R than their best twins remains the same (82%) and this amount is 70% when we consider all the pairs (14/20). Thus we confirm that the effect of inclination on $\Delta\lambda_R$ for the galaxies in our sample is small. It is noteworthy that the six pairs in which the AGN have smaller or equal λ_R than its twin(s) are all barred. For the unbarred twins, we continue having positive $\Delta\lambda_R$ in 100% of the pairs after deprojecting.

The stellar ages of the discs could also have an influence on λ_R since there is a relation between age and V/σ (the older the stellar population the lower V/σ and viceversa; e.g. van de Sande et al. 2018). In order to explore this possibility we characterised the stellar populations of the galaxies in the same region as λ_R via the code STECKMAP (Ocvirk et al. 2006a,b). We used a similar methodology as in dMC19. In Appendix C we show an alternative version of Fig. 2 indicating the differences in light-weighted averaged stellar age in different colours. In general, the discs of AGN are older than those of their twins (13/20; red symbols in Fig. C.1; see also Lacerda et al. 2020), whilst the other seven show equal or younger ages. The maximum differences are ±1.4 Gyr. This is the opposite of what we would expect if the differences in λ_R were driven by the differences in the stellar ages of their discs. We also note that for some AGN with more than one twin, the differences in stellar age are both positive and negative (e.g. NGC 1093, UGC 00005 and UGC 03973). This constitutes further indications that differences in stellar age are not driving our result. A detailed study of the stellar populations of these galaxies including the central regions will be the subject of a forthcoming work (del Moral-Castro, in prep.).

Another parameter that could have an influence on λ_R is the bulge fraction (Krajnović et al. 2013), with the larger the bulge-to-total flux ratios (B/T) the lower the λ_R. Although our twins are matched in Hubble type and M_* and in this work we compare λ_R in the region dominated by the disc, we evaluate whether possible differences in the B/T fractions might have any influence on our result. In Appendix C we show another version of Fig. 2 with different colours indicating the differences in B/T measured from SDSS r-band photometry (Méndez-Abreu et al. 2017). Nine active galaxies have higher B/T than their corresponding twins and 10 have lower values[2] (see Fig. C.2). Comparing galaxies with relatively large differences in effective radius (R_e) could also have an impact on $\Delta\lambda_R$. There are 8 AGN with higher R_e than their twins and 12 showing lower R_e. Considering only the 13 pairs with smaller R_e differences than 30% of the AGN R_e, we have 9/13 pairs (69%) having $\Delta\lambda_R > 0.1$ and 6/8 pairs (75%) if we only consider the best twins. Finally, galaxies with larger M_* generally have lower λ_R values (e.g. Veale et al. 2017). In our case, 10 AGN have larger M_* than their twins, and 10 have lower M_* (see Table 1). Thus, the differences in stellar λ_R are not driven by smaller bulge fraction, R_e, or M_* of the AGN relative to their twins.

The results presented in this work provide statistical support to the preliminary interpretation of our pilot study (dMC19). We identify the higher λ_R measured in the discs of isolated AGN as the imprint of the angular momentum transfer from the inflowing gas to the baryonic matter in the disc (Kormendy 2013; Saha & Jog 2014). A large-scale disc or bar instability would have induced gas to move from the disc to the central region, triggering nuclear activity. For this inflow to happen, the gas had to efficiently transfer angular momentum to the baryonic matter remaining in the disc to conserve the total angular momentum of the isolated system. As a consequence of this internal angular momentum redistribution, the galactic disc got dynamically colder (i.e. higher λ_R). In the case of the barred galaxies, both active and non-active, the bars promote the inflow of gas, transporting angular momentum outwards (e.g. Kormendy 2013). This makes it more challenging to detect differences in λ_R between twins than in the case of the non-barred galaxies.

Another possibility is that the gas has an external origin (i.e. minor mergers) in the case of the active galaxies. As we

---

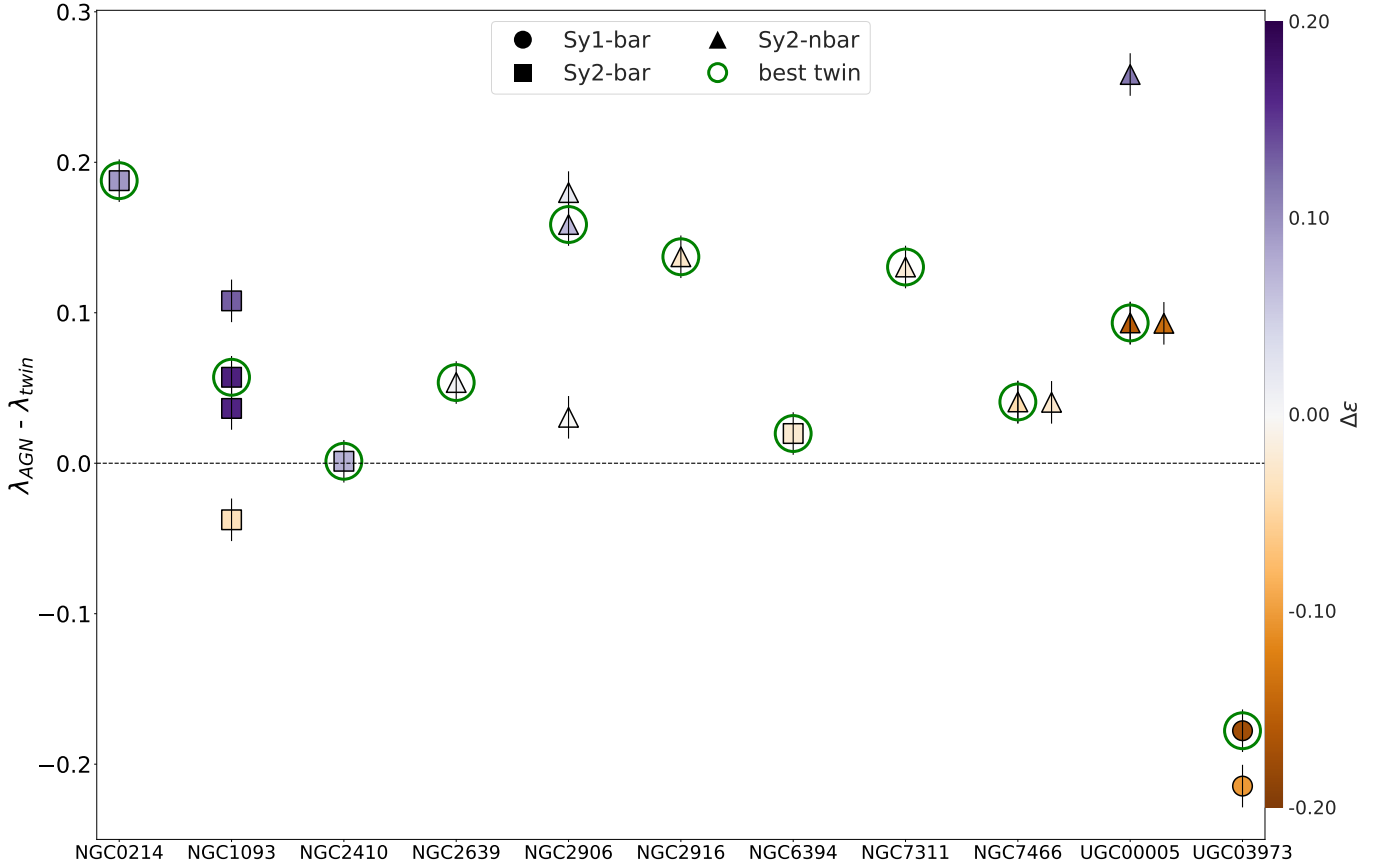[2] We note that NGC 2540 does not have B/T value (see Sect. 3).

Fig. 2. Differences in stellar λ_R between the pairs of twin galaxies. The best twin of each AGN is indicated with a green circle. Each column corresponds to an active galaxy and each symbol to the difference in λ_R with each of its twins. The colour code indicates the difference in ellipticity ($\epsilon_{AGN} - \epsilon_{twin}$, see Table 1). Error bars correspond to propagation of the individual uncertainties (see Sect. 3).

mentioned in Sect. 2, our sample does not include major mergers and clearly interacting systems, but based only on the SDSS images we cannot rule out the presence of minor mergers; see Smirnova et al. (2010) for a comparison between SDSS and deep optical images of apparently isolated Seyfert galaxies. Thus, gas-rich minor mergers constitute another possible explanation for the results presented in this work if they are prevalent in AGN: not only do these minor mergers promote spiral structure (Purcell et al. 2011) therefore increasing the disc λ_R, but they also provide gas supply that can potentially trigger nuclear activity (e.g. Neistein & Netzer 2014; Tadhunter et al. 2014). Deeper optical imaging is required to detect low surface brightness features indicative of merging activity (Ramos Almeida et al. 2011).

In the framework of these interpretations, it would also be relevant to look for differences between the actual specific angular momenta of the active and non-active twins. To do that we use j_*, the stellar specific angular momentum (Fall 1983; Romanowsky & Fall 2012; see Appendix D). To compare with λ_R, we computed j_* in the disc-dominated region and show the j_*–M_* diagram in Appendix D. We find that 50% of the pairs show positive/negative differences in j_*, and this is also valid if we calculate the total j_* values (i.e. including the bulge-dominated region). This would imply that AGN are triggered in discs in which a redistribution of angular momentum has happened (resulting in similar j_* and higher λ_R), but not necessarily in galaxies with higher/lower angular momentum or with higher/lower circular velocities (and thus more/less massive haloes). Nevertheless, we cannot rule out an underes-

timation of the j_* values calculated for our sample because of the limited field of view of the CALIFA data. According to Romanowsky & Fall (2012) at least $2\,R_e$ are necessary to estimate j_* reliably[3], and 16 out of the 25 galaxies in our sample have $R_{out} < 2\,R_e$.

Finding galaxy-scale differences between the active galaxies and their non-active twins appears puzzling because AGN are now understood as a short and likely episodic phase of galaxy evolution. The lifetimes of AGN are estimated to be $\leq 100\,$Myr (e.g. Martini 2004; Hopkins et al. 2005), which represents a tiny fraction of the time that any change in galaxy morphology and dynamics might take (e.g. Combes 2005; Lotz et al. 2008). Therefore, if all SMBHs go through an active phase we should not expect any large-scale difference between the twins. The result shown in Fig. 2 could then imply that not every galaxy goes through an active fase, at least in the redshift and mass range considered in this work.

This Letter shows, for the first time, tentative evidence that the discs of AGN in seemingly isolated spiral galaxies of intermediate stellar masses ($10^{10} < M_* < 10^{11}\,M_\odot$) present larger rotational support than their non-active twins. Performing one-to-one comparisons rather than the commonly used AGN versus control sample studies was fundamental to spot this. This result needs to be further explored and confirmed for a larger sample of active and non-active galaxies, preferably using integral field data of higher angular and spectral resolution and larger spatial coverage.

---

[3] This is not the case for λ_R, which is usually measured within $1\,R_e$.

References

Alexander, D. M., & Hickox, R. C. 2012, New Astron. Rev., 56, 93
Baldwin, J. A., Phillips, M. M., & Terlevich, R. 1981, PASP, 93, 5
Barrera-Ballesteros, J. K., Falcón-Barroso, J., García-Lorenzo, B., et al. 2014, A&A, 568, A70
Bundy, K., Bershady, M. A., Law, D. R., et al. 2015, ApJ, 798, 7
Cappellari, M. 2016, ARA&A, 54, 597
Cappellari, M. 2017, MNRAS, 466, 798
Cappellari, M., & Copin, Y. 2003, MNRAS, 342, 345
Cappellari, M., & Emsellem, E. 2004, PASP, 116, 138
Cappellari, M., Emsellem, E., Krajnović, D., et al. 2011, MNRAS, 413, 813
Cid Fernandes, R., Stasińska, G., Schlickmann, M. S., et al. 2010, MNRAS, 403, 1036
Colless, M. 2018, Proc. IAU, 14, 215
Combes, F. 2005, Sci. Am., 293, 42
Cortese, L., Fogarty, L. M. R., Bekki, K., et al. 2016, MNRAS, 463, 170
Croom, S. M., Lawrence, J. S., Bland-Hawthorn, J., et al. 2012, MNRAS, 421, 872
del Moral-Castro, I., García-Lorenzo, B., Ramos Almeida, C., et al. 2019, MNRAS, 485, 3794
Emsellem, E., Cappellari, M., Krajnović, D., et al. 2007, MNRAS, 379, 401
Emsellem, E., Cappellari, M., Krajnović, D., et al. 2011, MNRAS, 414, 888
Fabian, A. C. 2012, ARA&A, 50, 455

Falcón-Barroso, J., Bacon, R., Bureau, M., et al. 2006, MNRAS, 369, 529
Falcón-Barroso, J., Lyubenova, M., van de Ven, G., et al. 2017, A&A, 597, A48
Falcón-Barroso, J., van de Ven, G., Lyubenova, M., et al. 2019, A&A, 632, A59
Fall, S. M. 1983, IAU Symp., 100, 391
García-Benito, R., Zibetti, S., Sánchez, S. F., et al. 2015, A&A, 576, A135
García-Burillo, S., Combes, F., Schinnerer, E., Boone, F., & Hunt, L. K. 2005, A&A, 441, 1011
Graham, M. T., Cappellari, M., Li, H., et al. 2018, MNRAS, 477, 4711
Ho, L. C. 2008, ARA&A, 46, 475
Hopkins, P. F., Hernquist, L., Cox, T. J., et al. 2005, ApJ, 630, 716
Ilha, G. S., Riffel, R. A., Schimoia, J. S., et al. 2019, MNRAS, 484, 252
Kalinova, V., Colombo, D., Rosolowsky, E., et al. 2017, MNRAS, 469, 2539
Kewley, L. J., Dopita, M. A., Sutherland, R. S., Heisler, C. A., & Trevena, J. 2001, ApJ, 556, 121
Kormendy, J. 2013, in Secular Evolution in Disk Galaxies, eds. J. Falcón-Barroso, & J. H. Knapen, 1
Kormendy, J., & Ho, L. C. 2013, ARA&A, 51, 511
Krajnović, D., Alatalo, K., Blitz, L., et al. 2013, MNRAS, 432, 1768
Lacerda, E. A. D., Sánchez, S. F., Cid Fernandes, R., et al. 2020, MNRAS, 492, 3073
Lotz, J. M., Jonsson, P., Cox, T. J., & Primack, J. R. 2008, MNRAS, 391, 1137
Ma, C.-P., Greene, J. E., McConnell, N., et al. 2014, ApJ, 795, 158
Martini, P. 2004, in Coevolution of Black Holes and Galaxies, ed. L. C. Ho, 169
Méndez-Abreu, J., Ruiz-Lara, T., Sánchez-Menguiano, L., et al. 2017, A&A, 598, A32
Neistein, E., & Netzer, H. 2014, MNRAS, 437, 3373
Ocvirk, P., Pichon, C., Lançon, A., & Thiébaut, E. 2006a, MNRAS, 365, 46
Ocvirk, P., Pichon, C., Lançon, A., & Thiébaut, E. 2006b, MNRAS, 365, 74
Purcell, C. W., Bullock, J. S., Tollerud, E. J., Rocha, M., & Chakrabarti, S. 2011, Nature, 477, 301
Ramos Almeida, C., & Ricci, C. 2017, Nat. Astron., 1, 679
Ramos Almeida, C., Tadhunter, C. N., Inskip, K. J., et al. 2011, MNRAS, 410, 1550
Rembold, S. B., Shimoia, J. S., Storchi-Bergmann, T., et al. 2017, MNRAS, 472, 4382
Romanowsky, A. J., & Fall, S. M. 2012, ApJS, 203, 17
Saha, K., & Jog, C. J. 2014, MNRAS, 444, 352
Sánchez, S. F., Kennicutt, R. C., Gil de Paz, A., et al. 2012, A&A, 538, A8
Sánchez, S. F., García-Benito, R., Zibetti, S., et al. 2016, A&A, 594, A36
Sánchez, S. F., Avila-Reese, V., Hernandez-Toledo, H., et al. 2018, Rev. Mex. Astron. Astrofis., 54, 217
Sarzi, M., Falcón-Barroso, J., Davies, R. L., et al. 2006, MNRAS, 366, 1151
Smirnova, A. A., Moiseev, A. V., & Afanasiev, V. L. 2010, MNRAS, 408, 400
Storchi-Bergmann, T., & Schnorr-Müller, A. 2019, Nat. Astron., 3, 48
Tadhunter, C., Dicken, D., Morganti, R., et al. 2014, MNRAS, 445, L51
van de Sande, J., Scott, N., Bland-Hawthorn, J., et al. 2018, Nat. Astron., 2, 483
Veale, M., Ma, C.-P., Greene, J. E., et al. 2017, MNRAS, 471, 1428
Walcher, C. J., Wisotzki, L., Bekeraité, S., et al. 2014, A&A, 569, A1

Appendix A: SDSS images

Here we include the colour-composite SDSS images of our sample of active and non-active twin galaxies (Fig. A.1).
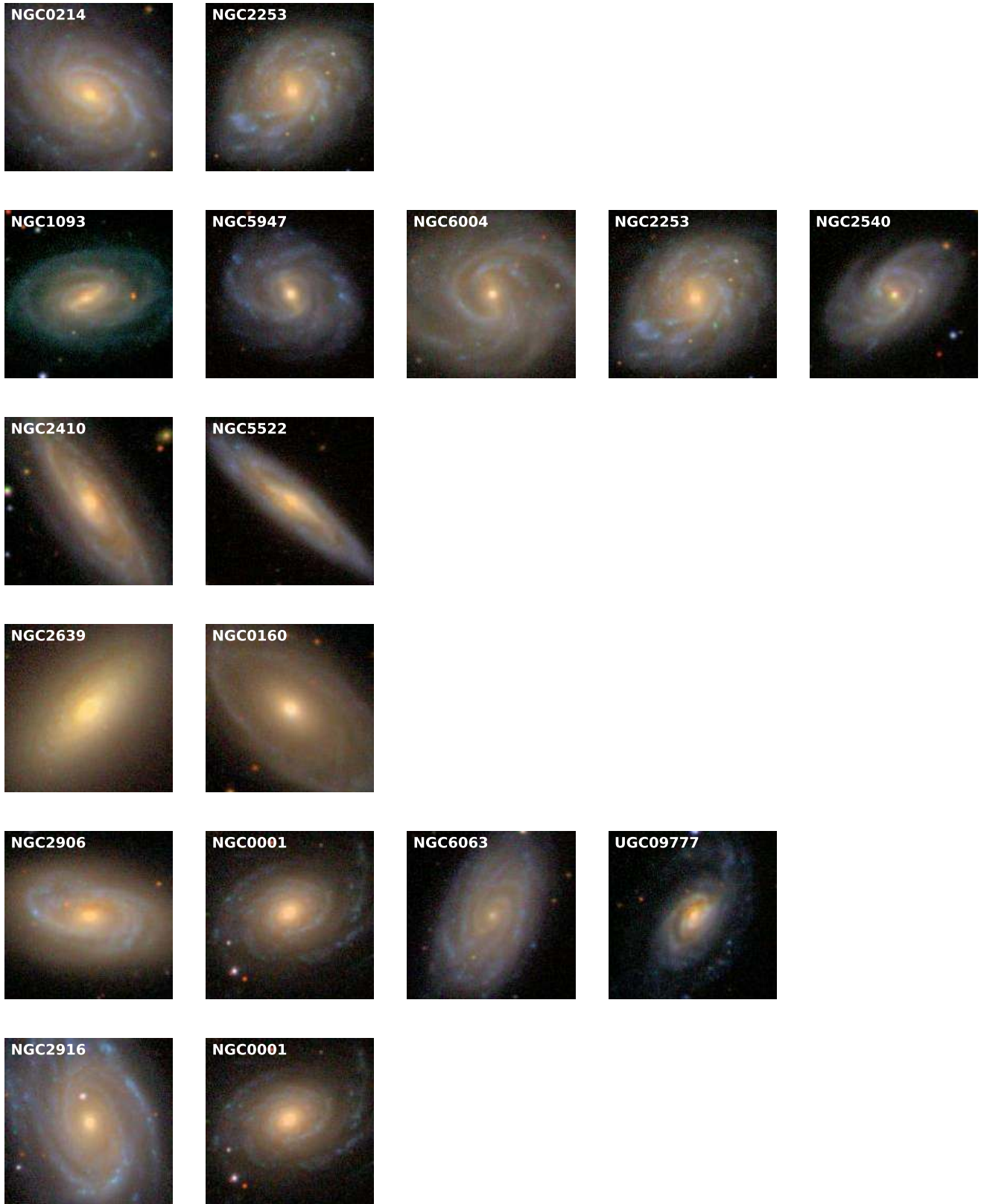
Fig. A.1. Colour-composite SDSS images of the active galaxies (*left column*) and their corresponding non-active twin(s). For AGN with more than one twin, the best twin is the one shown next to the AGN. Each image has a field of view of $90'' \times 90''$. North is up and east to the left.
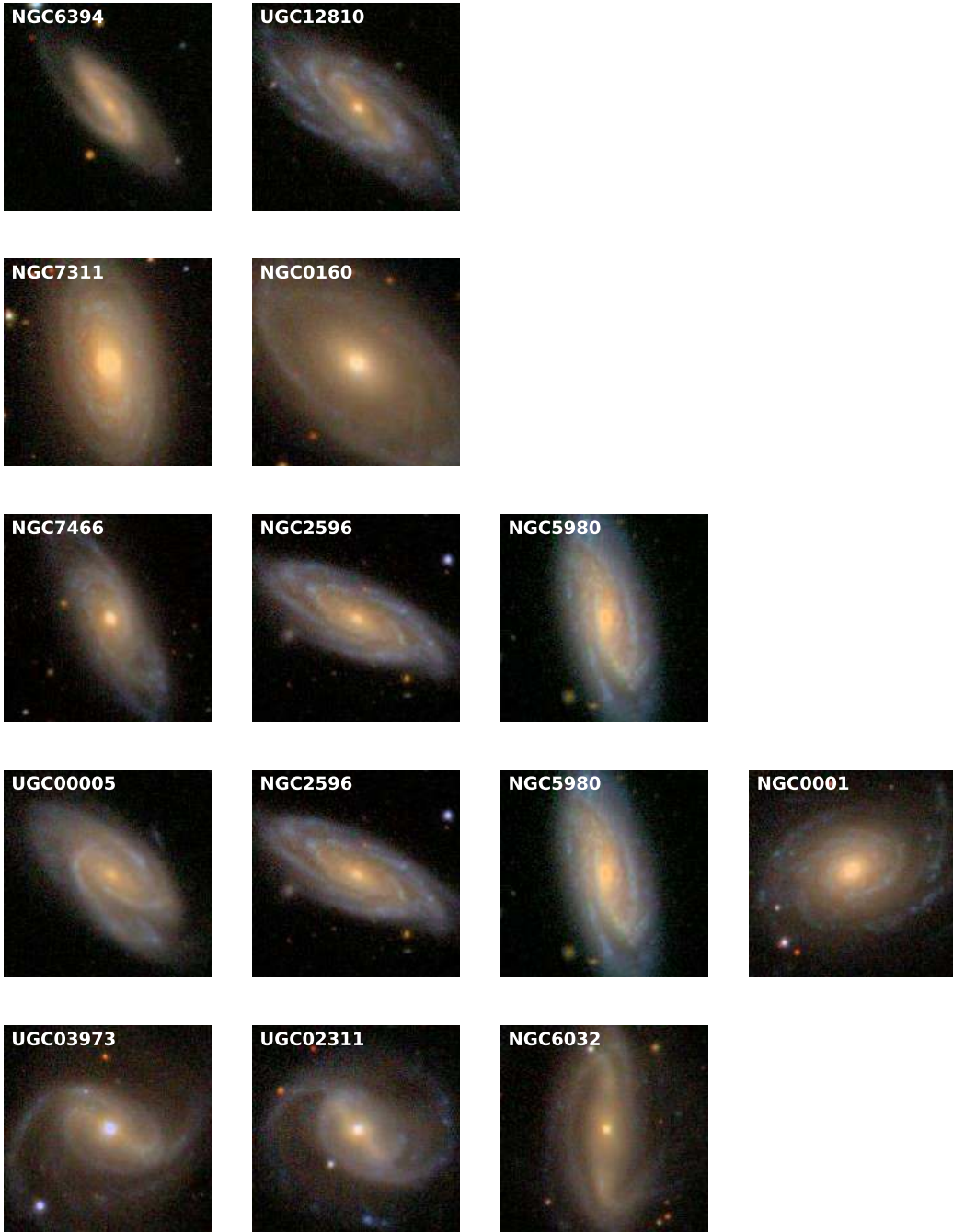
Fig. A.1. continued.

Appendix B: Deprojected λ_R values

To deproject the individual λ_R values we use the following equation from Appendix B of Emsellem et al. (2011):

$$\lambda_R^d = \frac{\lambda_R}{\sqrt{C^2 - \lambda_R^2(C^2 - 1)}},$$

(B.1)

where $C = \sin i / \sqrt{1 - \beta \cos^2 i}$, i the galaxy inclination, and β the anisotropy parameter. To estimate C for each galaxy we use the median value of β for its Hubble type ($\beta_{Sa} = 0.30$, $\beta_{Sb} = 0.34$, $\beta_{Sbc} = 0.29$ from Table B.1 in Kalinova et al. 2017). The individual λ_R^d are reported in Table 1. This deprojection introduces additional errors, including assumptions on internal galaxy dynamics. In an attempt to quantify this, we estimate conservative errors by taking into account the ellipticity errors from Méndez-Abreu et al. (2017), the statistical λ_R uncertainties, and the β standard deviation of the corresponding Hubble type.

Appendix C: Alternative figures

Here we include two alternative versions of Fig. 2, with different colours indicating differences in light-weighted averaged stel-

lar age (Fig. C.1) and in B/T from SDSS r-band photometry (Fig. C.2) between the twins.
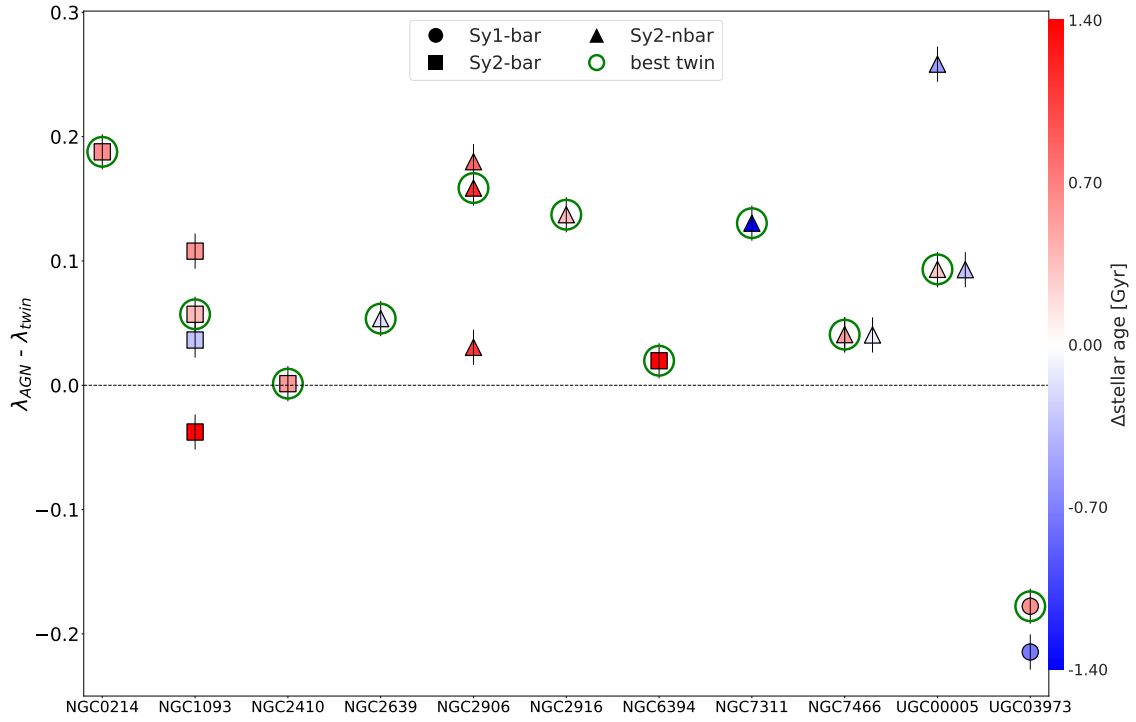

Fig. C.1. Same as Fig. 2 but with the colour code indicating differences in averaged luminosity-weighted stellar age measured in the same region as λ_R.
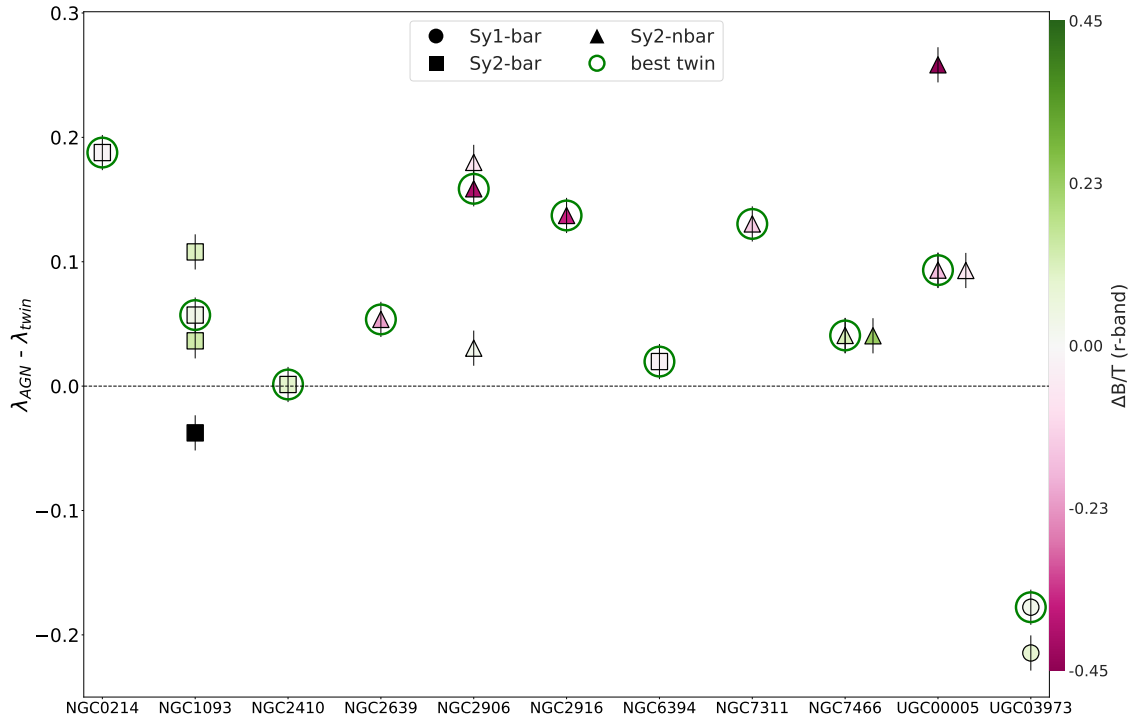

Fig. C.2. Same as in Fig. 2 but with the colour code indicating differences in B/T from SDSS r-band photometry (Méndez-Abreu et al. 2017). The best twin of each AGN is indicated with a red circle. NGC 2540 does not have B/T value reported in Méndez-Abreu et al. (2017) and thus its corresponding $\Delta\lambda_R$ appears as a black square.

Appendix D: Total specific angular momentum

To compute the j_* values of our galaxies as a proxy for the specific angular momentum (J), we use the methodology outlined by Romanowsky & Fall (2012) and adapted by Cortese et al. (2016) to IFS data as it follows

$$j_* = \frac{\sum_{i=1}^{N} F_i R_i |V_i|}{\sum_{i=1}^{N} F_i}, \tag{D.1}$$

where R_i, F_i, and V_i are the galactocentric radius, flux, and stellar velocity per spatial bin. We calculate the j_* values in the same region than λ_R (i.e. disc-dominated; see Sect. 3).

In Fig. D.1 we show the j_*–M_* diagram of the active and non-active galaxies in our sample. The scatter of this plot is strongly correlated with galaxy morphology (Fall 1983; Cortese et al. 2016), something that we also see for our galaxies, which include Sa, SBb, and S(B)bc types.
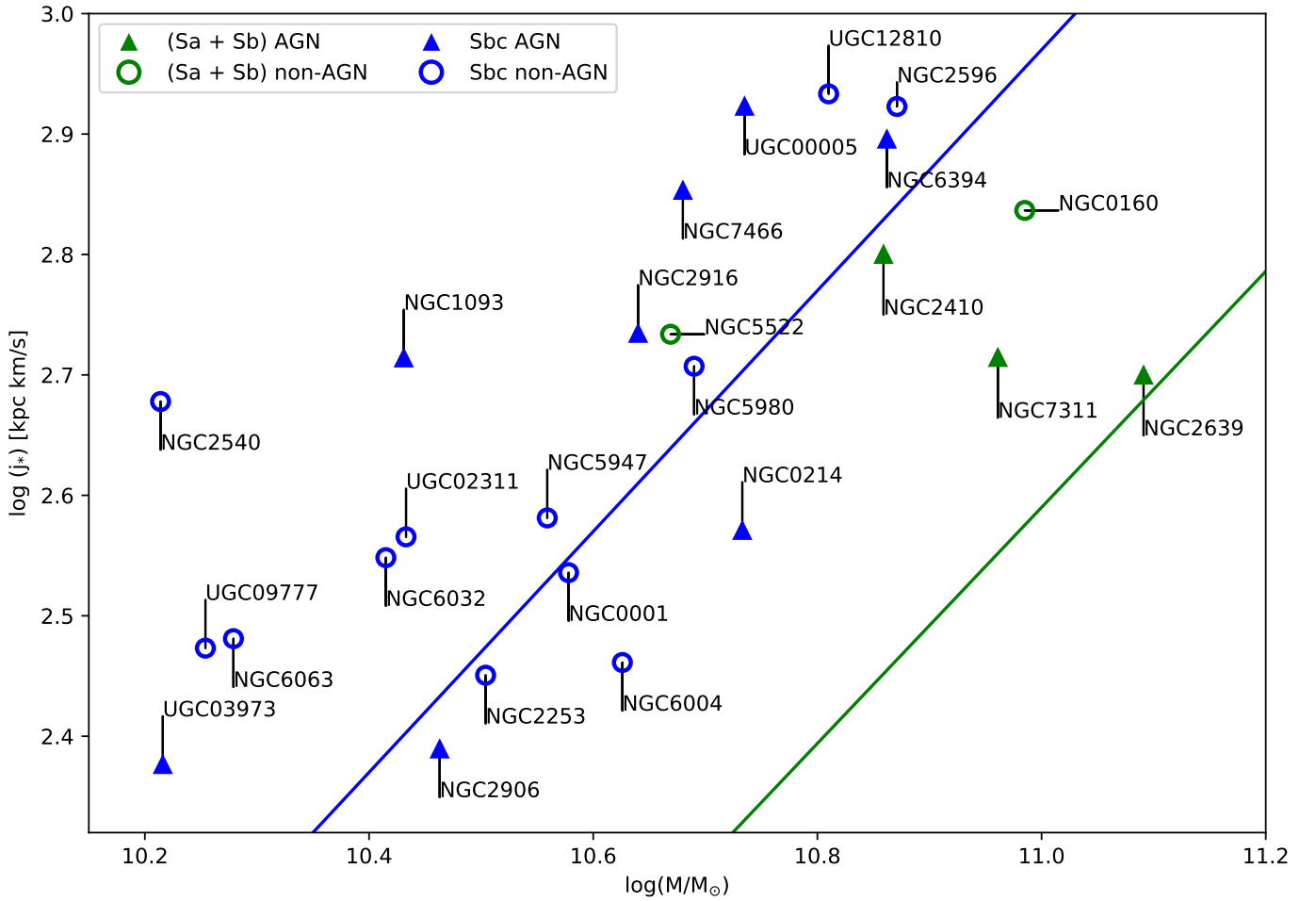

Fig. D.1. Active and non-active galaxies j_*–M_* diagram in our sample. The values of j_* corresponds to the disc-dominated region defined in Sect. 3. The filled symbols correspond to AGN and open symbols to non-active galaxies. The colours correspond to Hubble type (green to Sa and SBb and blue to S(B)bc galaxies). The green and blue lines correspond to the linear fits to S0/Sa-Sb and Sbc/later types from Cortese et al. (2016) within $1\,R_e$ for comparison.

Table D.1. j_* values for the sample.

AGN Twin (1)	log (j_*) (kpc km s^{-1}) (2)
NGC 0214	2.57
NGC 2253	2.45
NGC 1093	2.71
NGC 5947*	2.58
NGC 6004	2.46
NGC 2253	2.45
NGC 2540	2.68
NGC 2410	2.80
NGC 5522	2.73
NGC 2639	2.70
NGC 0160	2.84
NGC 2906	2.39
NGC 0001*	2.54
NGC 6063	2.48
UGC 09777	2.47
NGC 2916	2.73
NGC 0001*	2.54
NGC 6394	2.90
UGC 12810	2.93
NGC 7311	2.71
NGC 0160	2.84
NGC 7466	2.85
NGC 2596*	2.92
NGC 5980	2.71
UGC 00005	2.92
NGC 2596*	2.92
NGC 5980	2.71
NGC 0001*	2.54
UGC 03973†	2.38
UGC 02311*	2.57
NGC 6032	2.55

Notes. (1) Galaxy name as in Table 1, (2) j_* in the region dominated by the disc. * indicates the best twin of each AGN and † the only type 1 AGN in our sample.